Available online at www.sciencedirect.com

ScienceDirect

Nuclear Physics A 924 (2014) 1–23

NUCLEAR PHYSICS A

www.elsevier.com/locate/nuclphysa

Single and double beta decays in the $A = 100$, $A = 116$ and $A = 128$ triplets of isobars

J. Suhonen [a,*], O. Civitarese [b]

[a] *Department of Physics, P.O. Box 35 (YFL), FI-40014 University of Jyväskylä, Finland*
[b] *Department of Physics, University of La Plata, c.c. 67, (1900) La Plata, Argentina*

Received 15 November 2013; received in revised form 12 January 2014; accepted 14 January 2014

Available online 21 January 2014

Abstract

In this paper we analyze the ground-state-to-ground-state two-neutrino double beta ($2\nu\beta\beta$) decays and single EC and β^- decays for the $A = 100$ (^{100}Mo–^{100}Tc–^{100}Ru), $A = 116$ (^{116}Cd–^{116}In–^{116}Sn) and $A = 128$ (^{128}Te–^{128}I–^{128}Xe) triplets of isobars. We use the proton–neutron quasiparticle random-phase approximation (pnQRPA) with realistic G-matrix-derived effective interactions in very large single-particle bases. The purpose is to access the effective value of the axial-vector coupling constant g_A in the pnQRPA calculations. We show that the three triplets of isobars represent systems with different characteristics of orbital occupancies and cumulative $2\nu\beta\beta$ nuclear matrix elements. Our analysis points to a considerably quenched averaged effective value of $\langle g_A \rangle \approx 0.6 \pm 0.2$ in the pnQRPA calculations.

Keywords: Proton–neutron quasiparticle random-phase approximation; Two-neutrino double beta decays; Cumulative nuclear matrix elements; Single beta decays; Orbital occupancies; Renormalization of the axial-vector coupling constant

1. Introduction

Reliable calculation of the nuclear matrix elements (NMEs) related to the neutrinoless double beta ($0\nu\beta\beta$) decays of atomic nuclei is without doubt of paramount importance for extraction of quantitative information about the neutrino masses from the possible detection of this

* Corresponding author.
E-mail addresses: jouni.suhonen@phys.jyu.fi (J. Suhonen), osvaldo.civitarese@fisica.unlp.edu.ar (O. Civitarese).

0375-9474/$ – see front matter
http://dx.doi.org/10.1016/j.nuclphysa.2014.01.004

mode of weak decay [1,2]. Such calculations have been pursued mostly in the framework of the quasiparticle random-phase approximation (QRPA) [3], in particular in its proton–neutron variant (pnQRPA). A host of other models, ranging from the interacting shell model (ISM) to various mean field theories, have also been used in the calculations. The resulting NMEs have been analyzed in the review article [4]. The following are recently studied central issues in the calculations of the NMEs: (a) the role of the chosen single-particle valence space and orbital occupancies [5–7], (b) the role of shell-closure effects [4,8], (c) the role of deformation [9–12] and (d) the effective value of the axial-vector coupling constant $g_{\rm A}$ of weak interactions [13–17].

The various nuclear-structure aspects related to the $0\nu\beta\beta$ NME calculations can be conveniently studied in the context of the simpler two-neutrino double beta ($2\nu\beta\beta$) decays. The simplification is based on the facts that (i) the Gamow–Teller type of virtual transitions dominate the decay amplitude, (ii) the lowest virtual decays can be related to measured rates of single beta decays [18] and (iii) the associated half-lives have been measured for a number of $2\nu\beta\beta$-decaying nuclei [19]. Yet it has to be kept in mind that the momentum transfer of the $2\nu\beta\beta$ and $0\nu\beta\beta$ decays is rather different and may lead to qualitative differences between them.

In the case of the $2\nu\beta\beta$ decays the by far most popular model in use is the pnQRPA [3] or some renormalized versions of it [20–23]. Also the interacting shell model (ISM) has been very successful in $2\nu\beta\beta$ calculations, e.g. by predicting the $2\nu\beta\beta$-decay half-life of ^{48}Ca in [24], later verified by experiment in [25]; for a recent review see [26]. A particular problem with the pnQRPA calculations, not present in the ISM calculations, is the unsettled value of the particle–particle interaction parameter $g_{\rm pp}$ describing the strength of the proton–neutron interaction in the 1^+ channel. Since the introduction of this parameter [27,28] its values have been tried to fix by the inspection of the measured single-beta-decay rates [18,29] or $2\nu\beta\beta$ decay rates [30–33]. Contrary to these approaches, we make now an attempt to relate the values of $g_{\rm pp}$ to the values of $g_{\rm A}$ through the data on the $2\nu\beta\beta$ half-lives and beta-decay rates.

In the present article we touch the issues (a) and (d) mentioned above by analyzing the $2\nu\beta\beta$ and single beta decays by the pnQRPA method in the following three triplets of isobars, namely ^{100}Mo–^{100}Tc–^{100}Ru, ^{116}Cd–^{116}In–^{116}Sn and ^{128}Te–^{128}I–^{128}Xe. The double and single beta decays of these triplets are presented in Fig. 1. In these three cases the $2\nu\beta\beta$ decay proceeds from the even–even mother nucleus to the even–even grand-daughter ground state and the beta decays proceed from the 1^+ ground state of the intermediate odd–odd nucleus to the ground states of the neighboring even–even nuclei, electron capture (EC) decay to the left and β^- decay to the right. The associated experimental half-lives of the $2\nu\beta\beta$ decays and the comparative half-lives ($\log ft$ values) of the beta decays are given in the figures. Based on these data we analyze in this paper the possible quenching of the axial-vector coupling constant $g_{\rm A}$ for Gamow–Teller type of spin–isospin transitions. At the same time we investigate the basic nuclear-structure properties of the involved nuclei in terms of their orbital occupancies and fine structure of their $2\nu\beta\beta$ NMEs.

The article is organized as follows: In Section 2 the basic theoretical framework is briefly reviewed. In Section 3 the model-space aspects and adjustment of the model parameters are explained. In addition, the orbital occupancies of the key orbitals in the involved even–even nuclei are given. In Section 4 we associate the values of the parameter $g_{\rm pp}$ to the values of $g_{\rm A}$ and study the behavior of the fine structure of the $2\nu\beta\beta$ NMEs as functions of these parameters. In Section 5 an account of the investigations on the quenching of $g_{\rm A}$ is given and finally, in Section 6, we summarize and draw the conclusions.

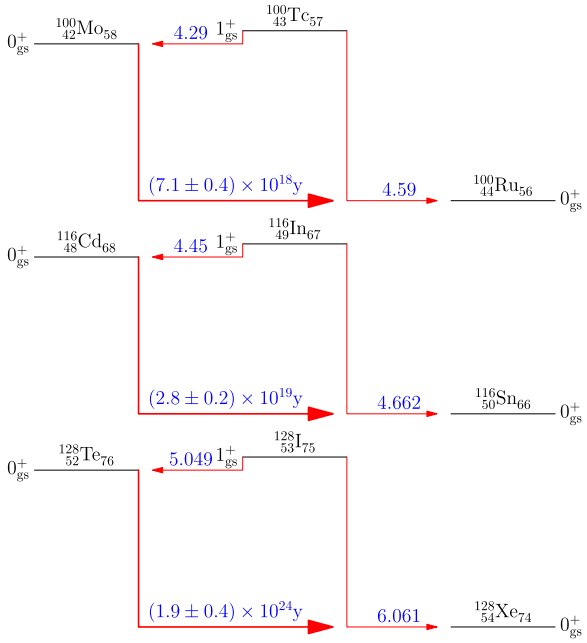

Fig. 1. Double and single beta decay characteristics of the presently studied triplets of isobars. The double-beta half-lives and log ft values of the single beta decays are given above the transition arrows.

2. Outline of theory

We begin by defining the comparative half-lives (log ft values) of the $1^+ \to 0^+$ Gamow–Teller transitions that are of interest in this work. The log ft value is defined as [34]

$$\log ft = \log\bigl(f_0 t_{1/2}[s]\bigr) = \log\left[\frac{6147}{B_{\rm GT}}\right], \quad B_{\rm GT} = \frac{g_{\rm A}^2}{3}\left|\bigl(0^+\|\sum_k t_k^{\pm}\boldsymbol{\sigma}_k\|1^+\bigr)\right|^2 \tag{1}$$

for the EC or β^- type of transitions. Here the half-life has been given in seconds to enable taking the logarithm and $t_k^{\pm}$ is the flavor-changing operator for the k-th nucleon in the EC or β^- direction and f_0 is the leptonic phase-space factor for the allowed EC or β^- decays as defined in [34].

The $2\nu\beta\beta$-decay half-life can be compactly written in the form

$$\bigl[t_{1/2}^{(2\nu)}\bigl(0_i^+ \to 0_f^+\bigr)\bigr]^{-1} = g_{\rm A}^4 G_{2\nu}\bigl|M^{(2\nu)}\bigr|^2, \tag{2}$$

where $g_{\rm A}$ is the weak axial-vector coupling constant and $G_{2\nu}$ stands for the leptonic phase-space factor without including $g_{\rm A}$ in a way defined in [35]. Values of these factors are listed in Table 1. The initial ground state is denoted by 0_i^+ and the final ground state by 0_f^+. The involved NME is written as

$$M^{(2\nu)} = \sum_m M^{(2\nu)}\bigl(1_m^+\bigr), \tag{3}$$

where

Table 1
Adopted values of the phase-space factors in (2). The values are taken from [35] and they are given in units of inverse years.

Triplet	$A = 100$	$A = 116$	$A = 128$
$G_{2\nu}$ (yr^{-1})	3.31×10^{-18}	2.76×10^{-18}	2.69×10^{-22}

$$M^{(2\nu)}\left(1_m^+\right) = \frac{M_{\rm F}(1_m^+) M_{\rm I}(1_m^+)}{[\frac{1}{2}(\Delta + E(1_m^+)) - M_i c^2]/m_{\rm e}c^2}, \tag{4}$$

and the involved transition amplitudes are

$$M_{\rm I}\left(1_n^+\right) = \left(1_n^+ \Big\| \sum_k t_k^- \boldsymbol{\sigma}_k \Big\| 0_i^+\right), \qquad M_{\rm F}\left(1_m^+\right) = \left(0_f^+ \Big\| \sum_k t_k^- \boldsymbol{\sigma}_k \Big\| 1_m^+\right). \tag{5}$$

In the case of the pnQRPA the expression (4) has to be written in the form

$$M^{(2\nu)}_{\rm RPA}\left(1_m^+\right) = \sum_n \frac{M_{\rm F}(1_m^+)\langle 1_m^+|1_n^+\rangle M_{\rm I}(1_n^+)}{D_m}, \tag{6}$$

where the quantity D_m is the energy denominator containing the average energy of the 1^+ states emerging from the two pnQRPA calculations, one for the initial nucleus and the other for the final nucleus. The denominator can thus be written as

$$D_m = \left(\frac{1}{2}\Delta + \frac{1}{2}\left[E\left(1_m^+\right) + \tilde{E}\left(1_m^+\right)\right] - M_i c^2\right) \Big/ m_{\rm e}c^2, \tag{7}$$

where Δ is the nuclear mass difference of the initial and final 0^+ ground states, $\tilde{E}(1_m^+)$ is the energy of the mth 1^+ state in a pnQRPA calculation based on the initial ground state, $E(1_m^+)$ the same for a calculation based on the final ground state and $M_i c^2$ is the mass energy of the initial nucleus. The quantity $\langle 1_m^+|1_n^+\rangle$ is the overlap between the two sets of 1^+ states written as

$$\left\langle 1_m^+|1_n^+\right\rangle = \sum_{pn}\left[X_{pn}^{1_m^+}\bar{X}_{pn}^{1_n^+} - Y_{pn}^{1_m^+}\bar{Y}_{pn}^{1_n^+}\right] \tag{8}$$

and it takes care of the matching of the corresponding states in the two sets of states based on the initial and final even–even reference nuclei. The amplitudes X and Y ($\bar{X}$ and $\bar{Y}$) come from the pnQRPA calculation starting from the final (initial) nucleus of the double beta decay.

3. Model spaces and parameters

In the present calculations we have adopted the no-core approach and have included all the single-particle states from the very bottom of a spherical Coulomb-corrected Woods–Saxon (WS) potential well with the standard parametrization of Bohr and Mottelson [36], optimized for nuclei near the line of beta stability. All bound states and a number of resonant states with small decay widths have been included in the calculations for both protons and neutrons. The single-particle orbitals numbered 25 for the $A = 100$ and $A = 128$ systems and 26 for the $A = 116$ system. Small modifications of the WS energies were done for ^{100}Mo, ^{100}Ru, ^{128}Te and ^{128}Xe at the vicinity of the proton and neutron Fermi surfaces to allow for a better reproduction of the one-quasiparticle type of spectra of the neighboring odd-A nuclei. In particular, the basis set 'EXPWS' of Ref. [37] was adopted for ^{100}Mo. All the used single-particle energies are reviewed in Table 2 for neutrons and in Table 3 for protons.

Table 2
Neutron single-particle energies of the mean-field orbitals (first column) for nuclei of interest in the present calculations. The energies are given in units of MeV.

Orbital	Single-particle energy in MeV					
	^{100}Mo	^{100}Ru	^{116}Cd	^{116}Sn	^{128}Te	^{128}Xe
$0s_{1/2}$	−39.07	−40.33	−39.28	−40.38	−39.18	−40.18
$0p_{3/2}$	−33.21	−34.43	−33.89	−34.95	−34.08	−35.05
$0p_{1/2}$	−32.29	−33.50	−33.12	−34.17	−33.40	−34.36
$0d_{5/2}$	−26.56	−27.74	−27.71	−28.73	−28.21	−29.15
$0d_{3/2}$	−24.43	−25.57	−25.90	−26.90	−26.60	−27.51
$1s_{1/2}$	−23.59	−24.72	−24.91	−25.90	−25.54	−26.45
$0f_{7/2}$	−19.31	−20.42	−20.92	−21.90	−21.73	−22.63
$0f_{5/2}$	−15.55	−16.59	−17.68	−18.61	−18.81	−19.67
$1p_{3/2}$	−15.36	−16.39	−17.09	−18.01	−18.01	−18.86
$1p_{1/2}$	−13.92	−14.92	−15.81	−16.71	−16.84	−17.67
$0g_{9/2}$	−11.58	−12.62	−13.63	−14.56	−14.75	−15.60
$1d_{5/2}$	−8.30	−8.19	−9.28	−10.11	−10.43	−11.19
$0g_{7/2}$	−4.50	−6.83	−8.66	−9.50	−10.23	−11.01
$2s_{1/2}$	−6.50	−6.39	−7.47	−8.22	−8.59	−9.30
$1d_{3/2}$	−5.80	−5.62	−6.98	−7.74	−8.27	−8.99
$0h_{11/2}$	−5.50	−6.50	−5.96	−6.83	−8.70	−9.40
$1f_{7/2}$	0.00	−0.60	−1.85	−2.52	−3.07	−3.72
$2p_{3/2}$	0.13	0.20	−0.83	−1.28	−1.69	−2.19
$1f_{5/2}$	2.72	2.17	0.92	0.46	−0.22	−0.74
$0h_{9/2}$	3.95	3.24	0.84	0.13	−1.08	−1.77
$0i_{13/2}$	4.72	3.90	1.96	1.18	0.30	−0.43
$2p_{1/2}$	5.72	6.43	−0.14	−0.46	−0.85	−1.26
$1g_{9/2}$	8.00	6.50	4.57	4.00	3.31	2.84
$0i_{11/2}$	10.60	10.60	10.20	9.65	8.08	7.55
$1g_{7/2}$	10.80	10.80	10.80	10.10	9.80	7.90
$2d_{5/2}$	–	–	5.01	4.51	7.62	8.56

Here it has to be noted that from the point of view of the present study such large model space is not necessary to describe the low-energy characteristics of the present nuclei. Also the properties of the Gamow–Teller giant resonance region do not need such a large number of single-particle states. The results for the single and double beta decays converge even when only the truly bound states, with negative single-particle energy, are included in the calculations. However, if e.g. the strength distribution of the isovector spin monopole excitations is studied, then such single-particle spaces, and even larger, are called for [38].

The Bonn-A G-matrix has been used as the starting point for the nucleon–nucleon interaction and it has been renormalized in the standard way [39,40]: The quasiparticles are treated in the BCS formalism and the pairing matrix elements are scaled by a common factor, separately for protons and neutrons. In practice these factors are fitted such that the lowest quasiparticle energies obtained from the BCS match the experimentally deduced pairing gaps for protons and neutrons respectively. The corresponding values of the pairing gaps and the resulting pairing strengths are cited in Table 4 for the nuclei of interest in this work. It should be noted, however, that applying the BCS approach to the $A = 128$ system is at the limits of applicability of this method due to the vicinity of the $Z = 50$ shell closure for Te [41]. Similar considerations concern the $A = 116$ system as well, ^{116}Sn being even semi-magic.

Table 3
Proton single-particle energies of the mean-field orbitals (first column) for nuclei of interest in the present calculations. The energies are given in units of MeV.

Orbital	Single-particle energy in MeV					
	^{100}Mo	^{100}Ru	^{116}Cd	^{116}Sn	^{128}Te	^{128}Xe
$0s_{1/2}$	−35.30	−33.37	−35.12	−33.40	−35.27	−33.67
$0p_{3/2}$	−29.74	−27.89	−30.07	−28.41	−30.53	−28.98
$0p_{1/2}$	−28.60	−26.76	−29.10	−27.44	−29.65	−28.11
$0d_{5/2}$	−23.26	−21.48	−24.09	−22.49	−24.86	−23.37
$0d_{3/2}$	−20.67	−18.92	−21.85	−20.26	−22.83	−21.34
$1s_{1/2}$	−19.57	−17.81	−20.54	−18.94	−21.40	−19.90
$0f_{7/2}$	−16.07	−14.37	−17.39	−15.85	−18.47	−17.03
$0f_{5/2}$	−11.54	−9.89	−13.43	−11.92	−14.86	−13.44
$1p_{3/2}$	−9.20	−8.00	−12.61	−11.10	−13.76	−12.33
$1p_{1/2}$	−7.50	−6.50	−11.06	−9.58	−12.33	−10.92
$0g_{9/2}$	−6.40	−6.70	−10.11	−8.63	−11.50	−10.11
$1d_{5/2}$	−2.81	−1.40	−4.56	−3.15	−5.94	−4.60
$0g_{7/2}$	−1.47	0.00	−4.03	−2.62	−5.91	−4.57
$2s_{1/2}$	−0.59	0.79	−2.19	−0.86	−3.46	−2.24
$1d_{3/2}$	0.20	1.60	−1.74	−0.40	−3.23	−1.97
$0h_{11/2}$	−0.11	1.41	−2.33	−0.94	−4.02	−2.70
$1f_{7/2}$	4.97	6.19	3.24	4.47	1.79	2.99
$2p_{3/2}$	6.25	7.42	5.18	6.17	4.16	5.18
$1f_{5/2}$	8.75	9.87	7.09	8.14	5.65	6.73
$0h_{9/2}$	9.10	10.40	6.04	7.32	3.79	5.04
$0i_{13/2}$	8.41	9.81	5.79	7.11	3.85	5.11
$2p_{1/2}$	7.80	9.80	6.37	7.37	5.43	6.38
$1g_{9/2}$	10.40	14.40	10.40	11.80	9.02	10.02
$0i_{11/2}$	15.40	17.40	14.20	15.40	12.00	13.40
$1g_{7/2}$	16.50	18.10	14.80	16.00	12.80	13.80
$2d_{5/2}$	–	–	9.00	10.20	7.00	8.00

Table 4
Values of pairing gaps for protons and neutrons (second and third columns), the values of the associated pairing strengths (fourth and fifth columns) and the value of the particle–hole strength parameter (last column) for the nuclei listed in the first column.

Nucleus	Δ_p (MeV)	Δ_n (MeV)	$g_{pair}^{(p)}$	$g_{pair}^{(n)}$	g_{ph}
^{100}Mo	1.374	1.255	0.895	0.865	0.90
^{100}Ru	1.484	1.400	0.875	0.895	0.90
^{116}Cd	1.477	1.373	0.941	0.889	1.00
^{116}Sn	–	1.159	0.941	0.817	1.00
^{128}Te	1.094	1.295	0.811	0.860	1.00
^{128}Xe	1.291	1.269	0.874	0.860	1.00

The wave functions of the 1^+ states of the intermediate nuclei have been produced by using the pnQRPA with the particle–hole and particle–particle degrees of freedom [27] included. The particle–hole and particle–particle parts of the proton–neutron two-body interaction are separately scaled by the particle–hole (g_{ph}) and particle–particle (g_{pp}) parameters. The particle–hole parameter affects the position of the Gamow–Teller giant resonance (GTGR) and its value was fixed by the available systematics [34] on the location of the resonance. The resulting values

Table 5
Occupancies of the proton and neutron orbitals close to the respective Fermi surfaces in the nuclei ^{100}Mo and ^{100}Ru.

Proton occupancies			Neutron occupancies		
Orbital	^{100}Mo	^{100}Ru	Orbital	^{100}Mo	^{100}Ru
$0f_{5/2}$	5.79	5.61	$1d_{5/2}$	5.32	3.16
$1p_{3/2}$	3.61	3.31	$2s_{1/2}$	0.70	0.20
$1p_{1/2}$	1.32	1.03	$1d_{3/2}$	0.66	0.30
$0g_{9/2}$	3.03	5.91	$0h_{11/2}$	1.03	1.24
$1d_{5/2}$	0.09	0.07	$0g_{7/2}$	0.46	1.48
$0g_{7/2}$	0.16	0.13			
$0h_{11/2}$	0.06	0.05			
$1d_{3/2}$	0.02	0.02			

Table 6
Occupancies of the proton and neutron orbitals close to the respective Fermi surfaces in the nuclei ^{116}Cd and ^{116}Sn.

Proton occupancies			Neutron occupancies		
Orbital	^{116}Cd	^{116}Sn	Orbital	^{116}Cd	^{116}Sn
$0f_{5/2}$	5.82	6.00	$1d_{5/2}$	5.54	5.57
$1p_{3/2}$	3.87	4.00	$0g_{7/2}$	6.96	7.02
$1p_{1/2}$	1.82	2.00	$2s_{1/2}$	1.33	1.05
$0g_{9/2}$	8.31	10.00	$1d_{3/2}$	2.02	1.27
$1d_{5/2}$	0.05	0	$0h_{11/2}$	2.17	1.14
$0g_{7/2}$	0.13	0	$1f_{7/2}$	0.07	0.04
$0h_{11/2}$	0.04	0	$2p_{3/2}$	0.01	0.006
$2s_{1/2}$	0.005	0	$2p_{1/2}$	0.005	0.002
$1d_{3/2}$	0.01	0	$0h_{9/2}$	0.07	0.04
			$1f_{5/2}$	0.02	0.01

of $g_{\rm ph}$ are listed in the last column of Table 4. The determination of the values of $g_{\rm pp}$, together with the determination of the values of the axial-vector coupling constant, are presented in Section 5.

At this point it is of interest to have a look at the occupancies of the relevant orbitals for the nuclei involved in the present calculations. The occupancy of a given orbital with total single-particle angular momentum j is obtained from the corresponding BCS occupation amplitude v_j by

$$\text{occupancy}(j) = (2j+1)v_j^2. \tag{9}$$

These occupancies are presented in Tables 5–7 for the nuclei under discussion in this work.

It should be stated that the present occupancies are based on the BCS approximation. A more consistent approach would be to compute the occupancies at the QRPA level. An attempt to this direction was done in [43] by the use of a self-consistent renormalized QRPA method (SRQRPA). In that work it was found for the $A = 76$ (Ge,Se) system that the differences between the BCS- and SRQRPA-predicted occupancies are generally small, except for some orbitals with large orbital angular momentum l, like $0g_{9/2}$, for which notable differences can sometimes occur. However, for $A = 128$ the vicinity of the $Z = 50$ shell closure makes the use of standard BCS

Table 7
Occupancies of the proton and neutron orbitals close to the respective Fermi surfaces in the nuclei ^{128}Te and ^{128}Xe. The experimental neutron occupancies for ^{128}Te were extracted from the data of [42].

Proton occupancies			Neutron occupancies			
Orbital	^{128}Te	^{128}Xe	Orbital	^{128}Te (th)	^{128}Te (exp)	^{128}Xe
$1d_{5/2}$	0.78	1.52	$1d_{5/2}$	5.63		5.52
$0g_{7/2}$	1.09	2.09	$0g_{7/2}$	7.34	8.00	7.15
$0h_{11/2}$	0.20	0.49	$0h_{11/2}$	9.20	8.66	8.06
$2s_{1/2}$	0.02	0.05	$2s_{1/2}$	1.41	1.28	1.23
$1d_{3/2}$	0.05	0.13	$1d_{3/2}$	2.40		2.04
			$1f_{7/2}$	0.06		0.07
			$2p_{3/2}$	0.01		0.01
			$0h_{9/2}$	0.08		0.09
			$2p_{1/2}$	0.004		0.004
			$1f_{5/2}$	0.02		0.02
			$1d_{3/2} + 1d_{5/2}$	8.03	7.94	7.56

questionable (since the protons are in the normal phase). Thus, we rely on the known systematics for single-particle energies and occupation factors and take them as phenomenological values.

The occupancies of the three isobaric triplets under discussion cover major shells that are configured in three different ways. Considering only occupancies of one particle or more, for the $A = 100$ nuclei, Mo and Ru, protons occupy orbitals up to and including the 1p–0f–$0g_{9/2}$ major shell and neutrons up to and including the orbitals $1d_{5/2}$, $0g_{7/2}$ and $0h_{11/2}$. For the $A = 116$ nuclei, Cd and Sn, protons occupy orbitals up to and including the 1p–0f–$0g_{9/2}$ major shell (as in the case of $A = 100$) and neutrons up to and including the 1d–2s–0g–$0h_{11/2}$ major shell. For the $A = 128$ nuclei, Te and Xe, protons occupy orbitals up to and including the $0g_{7/2}$ and $1d_{5/2}$ orbitals whereas neutrons occupy the complete 1d–2s–0g–$0h_{11/2}$ major shell (as in the case of $A = 116$).

Comparison of the occupancies of Tables 5–7 with experimental data would be extremely interesting. Such a comparison has been done for the $A = 76$ double beta system (^{76}Ge decaying to ^{76}Se) e.g. in [5–7] since experimental information about the proton and neutron occupancies is available [44,45]. A comparison for the $A = 130$ system was very recently performed in the experimental paper [42]. In that article also the neutron vacancies in ^{128}Te were given. The corresponding occupancies have been listed in the second last column of Table 7. It has to be noted that in [42] only the combined vacancy for the 1d orbitals is given. Comparing the corresponding calculated and experimental occupancies of Table 7 one notices that the agreement for the 1d and $2s_{1/2}$ orbitals is good. In the calculations the occupancy of the $0g_{7/2}$ orbital is depleted a bit while in experiment the orbital is full. Furthermore, in theory the $0h_{11/2}$ orbital seems to host an extra half a neutron that is coming from the depletion of the occupancy of the $0g_{7/2}$ orbital.

4. Double-beta properties of the studied nuclei

For each of the three studied nuclear systems, $A = 100, 116, 128$, one can perform an analysis of the behavior of the corresponding $2\nu\beta\beta$ NME in several different ways. We can start by creating a sample of the NMEs by starting from a given value of g_A and then extracting, by using this value of g_A, the experimental value of the $2\nu\beta\beta$ NME. We then fix the value of the particle–particle strength parameter g_{pp} by reproducing the value of the just extracted experimental NME

Table 8
Correspondence between the values of g_A and g_{pp} in the studied three isobaric triplets.

	$A = 100$		$A = 116$		$A = 128$	
g_A	g_{pp}	NME	g_{pp}	NME	g_{pp}	NME
1.25	0.868	0.132	0.855	0.073	0.755	0.028
1.00	0.857	0.206	0.834	0.114	0.748	0.044
0.80	0.829	0.322	0.788	0.178	0.735	0.069
0.70	0.790	0.421	0.725	0.232	0.723	0.090
0.60	0.610	0.573	0.455	0.316	0.701	0.123

in a pnQRPA calculation using this particular value of g_{pp}. In this way we create a one-to-one correspondence between the values of g_A and g_{pp}. This correspondence is presented in Table 8 for the studied three isobaric triplets.

As can be seen in Table 8 the values of g_A and g_{pp} correlate perfectly such that increasing value of g_{pp} corresponds to increasing value of g_A. One can, in addition, study the behavior of the $2\nu\beta\beta$ NMEs as functions of the parameter g_{pp}. This has been done in Fig. 2 for the three cases under discussion. Comparing the ranges of NMEs in Table 8 and the curves in Fig. 2 one realizes that the experimental magnitudes of the NMEs are achieved within a very small interval of g_{pp} values for the $2\nu\beta\beta$ decays of ^{100}Mo and ^{128}Te whereas for ^{116}Cd a much wider g_{pp} interval is required. This stems from the fact that in the region of interest the $2\nu\beta\beta$ NME is a very flat function of g_{pp} for ^{116}Cd.

For ^{100}Mo and ^{116}Cd the NME curves are quite steep for $g_{pp} > 0.7$ indicating that the collapse point of the pnQRPA is approaching. In fact, the NME collapses at about $g_{pp} \approx 0.8$ for ^{128}Te and at about $g_{pp} \approx 0.9$ for ^{100}Mo and ^{116}Cd. Near a collapse point the ground-state correlations of the pnQRPA grow too strong and the basic QRPA premise of small-amplitude collective motion is lost. Thus, being too close to the collapse point can produce unphysical results. In the present case the g_{pp} regions of interest, indicated in Table 8, are safe regions and the ground-state correlations do not enhance the backward-going amplitudes of the pnQRPA too much. In fact, as can be seen later in this paper, the g_{pp} regions of interest for $A = 116, 128$ are far from the collapse point and only for $A = 100$ the relevant region of g_{pp} is in the neighborhood of the collapse point but still at safe distance from it.

To have an idea how the NMEs of Table 8 are built state by state we show in Figs. 3 and 4 the cumulative sums of the NMEs for the isobaric triplets of interest and for the g_{pp} values indicated in Table 8. The cumulative sums are defined as

$$M^{(2\nu)}(K) = \sum_{k=1}^{K} M^{(2\nu)}\left(1_k^+\right), \tag{10}$$

where K is the upper limit in state number up to which the summing in Eq. (3) is to be carried out. Since E_K corresponds to the excitation energy of the last included 1^+ state in the sum the cumulative sum can be presented as a function of the excitation energy E_K in the odd–odd intermediate nucleus.

As can be seen in the left panel of Fig. 3 the cumulative sum for the $A = 100$ system is qualitatively the same up to $g_{pp} = 0.790$ ($g_A = 0.70$) but then flattens out for smaller values of g_{pp}. In all cases the first 1^+ state gives the dominant contribution and beyond it there are smaller canceling contributions up to about 10 MeV of excitation energy. For the very low values of g_{pp}

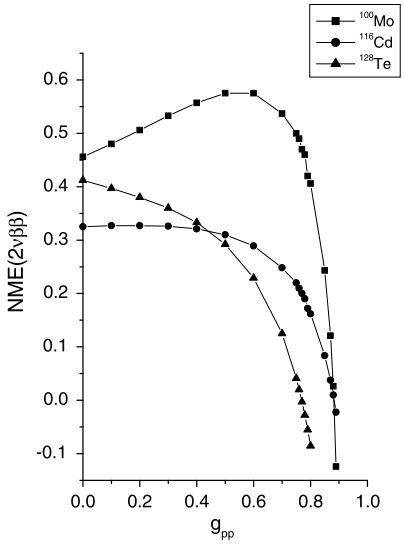

Fig. 2. The $2\nu\beta\beta$ NMEs as functions of the particle–particle interaction strength parameter $g_{\rm pp}$.

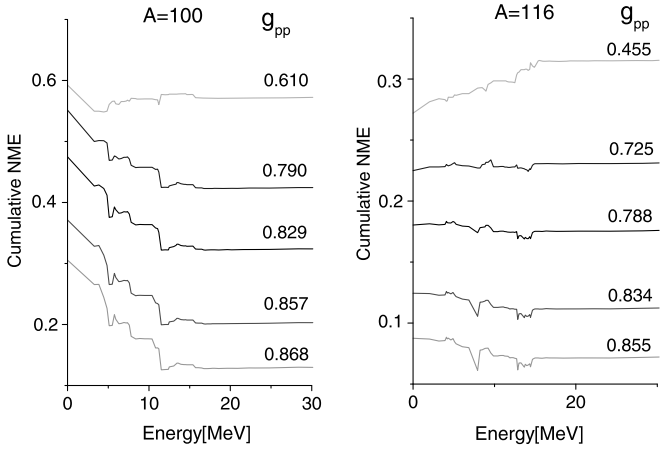

Fig. 3. Cumulative sums for the $2\nu\beta\beta$ NMEs of the $A = 100$ (left panel) and $A = 116$ (right panel) isobaric triplet as functions of the 1^+ excitation energy in ^{100}Tc and ^{116}In for five values of the interaction strength parameter $g_{\rm pp}$.

(or of $g_{\rm A}$) the cancellation effect seems to disappear and essentially a single-state dominance (SSD) situation is achieved [46,47]. On the other hand, for the $A = 116$ system of isobars the cumulative sum shows SSD down to rather low values of $g_{\rm pp}$ ($g_{\rm A}$), as seen in the right panel of Fig. 3. However, even for the very low values of $g_{\rm pp}$ ($g_{\rm A}$) the deviation from the SSD is quite small.

The structure of the cumulative sum for the decay of ^{128}Te is the most interesting one, as shown in Fig. 4. Judging by the similarity of the value of the contribution of the first 1^+ state and the value of the saturated NME at high excitation energy one could think that again one has a situation of SSD at hand. However, in the region between 3 MeV and 12 MeV one has strong contributions which cancel each other in the end. This pattern persists for values $g_{\rm pp} > 0.74$

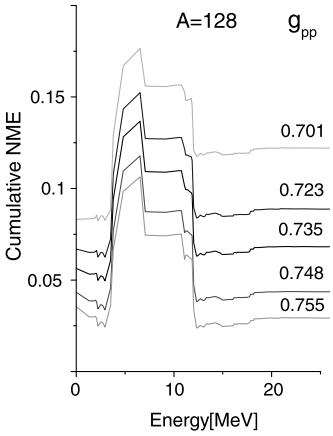

Fig. 4. Cumulative sums for the $2\nu\beta\beta$ NMEs of the $A = 128$ isobaric triplet as functions of the 1^+ excitation energy in ^{128}I for five values of the interaction strength parameter $g_{\rm pp}$.

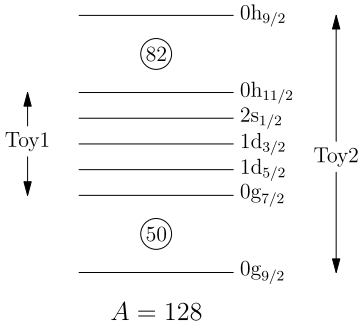

Fig. 5. Definition of the two toy bases Toy1 and Toy2 for the $A = 128$ isobaric triplet.

($g_{\rm A} > 0.8$). For $g_{\rm pp} < 0.74$ ($g_{\rm A} < 0.8$) the situation changes and the final value of the $2\nu\beta\beta$ NME is notably larger than the contribution coming from the first 1^+ state. Also the cancellation effect becomes weaker and disappears finally, leaving a sort of step at about 4 MeV of excitation. To shed further light to this situation we have examined the cumulative sum in smaller single-particle spaces, called toy model 1 and toy model 2 (Toy1 and Toy2 in Fig. 5) defined as

$$\begin{aligned} &\text{Toy1 basis:} \quad 2s_{1/2}, 1d_{3/2}, 1d_{5/2}, 0g_{7/2}, 0h_{11/2}, \\ &\text{Toy2 basis:} \quad \text{Toy1 basis} + 0g_{9/2} + 0h_{9/2}. \end{aligned} \tag{11}$$

These toy bases are also depicted in Fig. 5.

In the left panel of Fig. 6 we depict the cumulative sum computed in the Toy1 basis. Since the model space is now restricted to only one major shell the corresponding values of $g_{\rm pp}$ are larger than for the calculations in the full single-particle space in Fig. 4. However, the corresponding values of $g_{\rm A}$ are the same in both cases. The effect of the size of the single-particle space on model parameters was studied in detail in [6,7]. As can be seen in the left panel of Fig. 6 there is a setting in of strong contributions to the cumulative sums in the energy region starting from 3 MeV. From the right panel of Fig. 6 we notice that activation of the spin–orbit partners $0g_{9/2}$

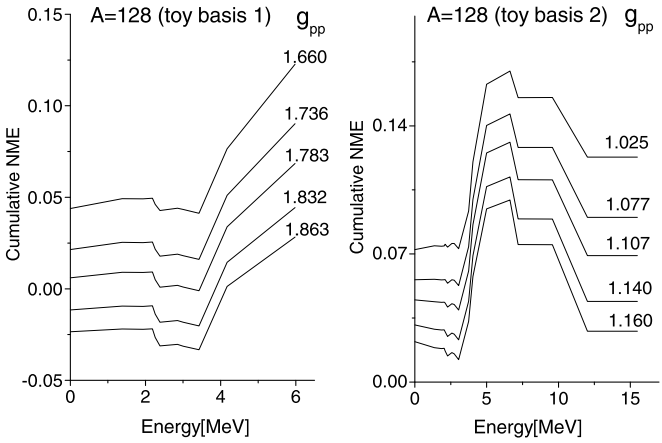

Fig. 6. Cumulative sums for the $2\nu\beta\beta$ NMEs of the $A = 128$ isobaric triplet as functions of the 1^+ excitation energy in ^{128}I for five values of the interaction strength parameter $g_{\rm pp}$. The toy models Toy1 (left panel) and Toy2 (right panel) of (11) have been used in the calculations.

and $0h_{9/2}$ of the orbitals $0g_{7/2}$ and $0h_{11/2}$ shifts the cumulative sums to larger values as a whole and adds the negative contributions canceling the strong contributions built in the Toy1 basis. The final pattern of the cumulative sums in the Toy2 basis is then close to the pattern encountered in Fig. 4 for the full basis. This feature is a strong evidence of the importance of including all the spin–orbit partners in the $2\nu\beta\beta$-decay calculations. This was pointed out earlier in the context of $0\nu\beta\beta$-decay calculations in [6,7].

The conclusions of the above study of the role of the spin–orbit partners in building the $2\nu\beta\beta$ NME differs notably from the conclusions drawn based on the study of the intermediate 1^+ contributions to the NME of the ^{128}Te decay in [48]. There calculations were done by the use of the IBA model and its extensions to include both bosonic and fermionic degrees of freedom in building the wave functions of the $2\nu\beta\beta$ initial, intermediate and final states. A single-particle basis corresponding to the present Toy1 basis was used in the calculations and practically a SSD pattern of the cumulative $2\nu\beta\beta$ NME was obtained. A claim was made that most probably the left out spin–orbit partners do not alter the situation because of the weak right leg of the intermediate transitions [48]. Contrary to this, in the present calculations notable 1^+ contributions between 3 MeV and 12 MeV have been recorded. It should further be noted that these contributions arise from states that reside below the Gamow–Teller giant resonance region. The above-mentioned contradictory features between the two calculations are highly interesting and merit further studies in the future.

5. Quenching of the effective value of $g_{\rm A}$

In this section we study the possible quenching of the values of the axial-vector coupling constant $g_{\rm A}$ in model calculations using the pnQRPA approach. The present study is complementary to the earlier work of [18] which discussed the incompatibility of the pnQRPA-computed $2\nu\beta\beta$-decay and single-beta-decay half-lives for the same nuclei and for the typical values $g_{\rm A} = 1.00$–1.25 of the axial-vector coupling constant.

Table 9
Extracted values of g_{pp} and g_A for the three discussed isobaric chains. For comparison are shown the effective values of g_A obtained in the IBFFM-2 and IBA-2 theory frameworks. In the last column SSD = single-state dominance and CA = closure approximation.

A	This work			IBFFM-2 [48]		IBA-2 [15]
	g_{pp}	$g_A(\beta)$	$g_A(\beta\beta)$	$g_A(\beta)$	$g_A(\beta\beta)$	$g_A(\beta\beta)$
100	0.820–0.838	0.61–0.70	0.75–0.85	–	–	0.46(1) [SSD]
116	0.440–0.616	0.66–0.81	0.59–0.65	–	–	0.41(1) [SSD]
128	0.524–0.532	0.330–0.335	0.38–0.43	0.25–0.31	0.293	0.55(3) [CA]

5.1. *Effective value of g_A from β and $\beta\beta$ decays*

The most ambitious aim would be to find three sets of values of g_A and g_{pp} in such a way as to reproduce the three sets of $2\nu\beta\beta$- and beta-decay data depicted in Fig. 1. As already mentioned in the introduction, in these three cases the $2\nu\beta\beta$-decay half-life is known, as also the comparative half-lives (log ft values) of the electron capture (EC) decay on the left and of the β^- decay on the right.

We can start by the procedure of Section 4, i.e. we start from a given value of g_A and then extract, by using this value of g_A, the experimental value of the $2\nu\beta\beta$ NME. We then fix the value of the particle–particle strength parameter g_{pp} in such a way that by using this g_{pp} the pnQRPA calculation reproduces the value of the extracted experimental NME. In this way we create a one-to-one correspondence between the values of g_A and g_{pp} shown in Table 8. The next question is whether we can reproduce the log ft values of the EC and β^- decays by any pair (g_A, g_{pp}). In [16] it was shown that this is almost possible, but not quite.

Next one can relax the constraints a bit and ask if one can find three sets of values (g_A, g_{pp}) such that the log ft values of the EC and β^- decays of the three cases $A = 100, 116, 128$ are reproduced. It now turns out that indeed such triple of pairs can be found leading to three sets of values $(g_A(\beta), g_{pp}(\beta))$. With the obtained value of $g_{pp}(\beta)$ one can evaluate the $2\nu\beta\beta$ NME in a pnQRPA calculation and then demand that this NME corresponds exactly to the experimental NME extracted by using an other effective value of the axial-vector coupling constant, coined $g_A(\beta\beta)$.

To follow the above described procedure one has to use the latest data on the involved single and double beta decays. The β^- decays have been measured quite accurately (see [49]) as visible in Fig. 1. The EC decays pose a problem since they have not been measured as accurately because of the involved small branchings to the electron-capture channels. For the decay transition $^{100}\text{Tc} \to {}^{100}\text{Mo}$ there is a recently measured value for the comparative half-life of $\log ft = 4.29^{+0.08}_{-0.07}$ [50], and for the transition $^{116}\text{In} \to {}^{116}\text{Cd}$ Ref. [51] gives $ft = [2.84 \pm 0.51(\text{stat}) \pm 0.45(\text{syst})] \times 10^4$ s. For the transition $^{128}\text{I} \to {}^{128}\text{Te}$ Ref. [52] gives $\log ft = 5.049(7)$. We have to take into account also the error bars of the measured $2\nu\beta\beta$ half-lives. From Ref. [19] we obtain the half-lives $(7.1 \pm 0.4) \times 10^{18}$ yr ($A = 100$), $(2.8 \pm 0.2) \times 10^{19}$ yr ($A = 116$) and $(1.9 \pm 0.4) \times 10^{24}$ yr ($A = 128$).

Combining the above listed log ft values and $2\nu\beta\beta$ half-lives, with their error bars included, one can derive the ranges of values of g_{pp}, $g_A(\beta)$ and $g_A(\beta\beta)$ listed in columns 2–4 of Table 9 and shown pictorially in Fig. 7. It should be noted here that the results for the $A = 100$ case deviate from those of our previous publication [16] since in the present work we use a more recent experimental result from [50] for the EC branch of beta decay. As can be seen in the

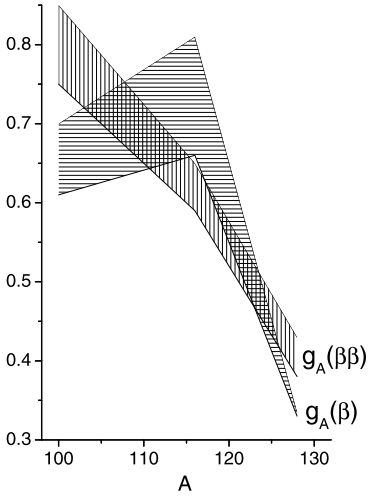

Fig. 7. Ranges of $g_{\rm A}(\beta)$ and $g_{\rm A}(\beta\beta)$ extracted in this work.

figure the values of $g_{\rm A}(\beta\beta)$ are monotonically decreasing whereas the values of $g_{\rm A}(\beta)$ behave irregularly.

The comparison between theoretical and experimental ft values, to estimate renormalization effects for β-decay moments, was used long ago to extract effective values of the axial-vector coupling constant. A very concrete example is given by the analysis of first-forbidden transitions around ^{208}Pb carried out in Ref. [36] in Chapter 3, page 353. Assuming some dominant single-particle configurations around the double-closed shell in $A = 208$, the analysis of Bohr and Mottelson yields two sets of values for the axial-vector coupling which are absolutely compatible with our present results, that is: $g_{\rm A}^{\rm eff}/g_{\rm A} = 0.5$ and $g_{\rm A}^{\rm eff}/g_{\rm A} = 0.7$. In fact, these values lie in the range of values depicted in Fig. 7, a feature which seems to indicate a sort of universality of the underlying renormalization. The result clearly supports our claim that the renormalization of single and double beta-decay transitions, for the two-neutrino mode, must be of the same nature, since the two decays participant in the $2\nu\beta\beta$ processes are not linked by a neutrino propagator.

A strong quenching of $g_{\rm A}(\beta) \sim 0.6$ was reported also in the shell-model calculations in the mass $A = 90$–97 region in Ref. [53]. This is very close to the presently obtained value $g_{\rm A}(\beta) = 0.61$–0.70 for the $A = 100$ case in Table 9. In a more recent shell-model study [26] values of about $g_{\rm A}(\beta\beta) \sim 0.7$ were obtained in the mass region $A = 128, 130$ and even a stronger quenching $g_{\rm A}(\beta\beta) = 0.56$ for $A = 136$. These are still weaker quenchings than the ones obtained for $A = 128$ in the present study (see Table 9). Here it should be mentioned that in the analyses of beta decays in the sd shell [54] and pf shell [55] only moderately quenched values $g_{\rm A}(\beta) \sim 1$ were used. However, from the results of [55] one can infer that for the transitions $0^+ \to 1^+$ a stronger quenching $g_{\rm A}(\beta) \sim 0.7$–$0.8$ would be needed in order to reproduce the corresponding experimental values.

In [12] several double-beta-decaying nuclei were analyzed by using a Gogny-interaction-based energy density functional approach. The individual 1^+ states of the intermediate nuclei could not be constructed but the total β^- and β^+/EC Gamow–Teller strengths could be generated. The available experimental total strengths could be reproduced quite nicely by using the unquenched value $g_{\rm A}(\beta) = 1.25$. However, these calculations cannot address the question about the need to quench the Gamow–Teller contribution to the lowest 1^+ transition.

Another interesting analysis of the quenching was done in [13] where both the beta-decay and $2\nu\beta\beta$ decay data were analyzed for the $A = 100, 116$ systems in the framework of the pnQRPA using least squares to achieve best-fit values for $g_{\rm A}$. In [13] the best fit values $g_{\rm A} = 0.74$ ($A = 100$) and $g_{\rm A} = 0.84$ ($A = 116$) were obtained. The first value touches the presently obtained range for $g_{\rm A}(\beta\beta)$ and the latter one is very close to the present range of values for $g_{\rm A}(\beta)$. So it seems that in the fitting of [13] the value of $g_{\rm A}$ for $A = 100$ is double-beta-like and for $A = 116$ more single-beta-like. Furthermore, it is interesting to note that in the first version [56] of the paper [13] also results for the $A = 128$ system were included. There the result $g_{\rm A} = 0.39$ was quoted which agrees with the range $g_{\rm A}(\beta\beta) = 0.38$–$0.43$ obtained in the present study. Hence, the $A = 128$ result of [56] is double-beta-like.

It should be noted that in terms of the pnQRPA calculations the present and the ones of [13, 56] are very similar as evidenced by comparing Fig. 2 of the present work with Fig. 1 of [13] and [56]. However, in [13,56] the adopted experimental data for the EC branches of decay were older than the data used in the present analysis: The log ft values 3.96 ($A = 100$) and 4.39 ($A = 116$) were adopted instead of 4.29 ($A = 100$) and 4.45 ($A = 116$) used in this work (see Fig. 1). Since the decay rate of the EC branch is very slowly varying in the pnQRPA calculations this can cause notable deviations in the best-fit values of $g_{\rm pp}$ and $g_{\rm A}$.

A monotonic behavior of $g_{\rm A}(\beta\beta)$ was parametrized in [15] by analyzing the magnitudes of NMEs produced by the IBA-2 and the interacting shell model (ISM). In this study the obtained $g_{\rm A}$-versus-A slope was very flat whereas in the present calculations the slope turns out to be steeper, as visible in Fig. 7. The contrast between the various calculations was shown in Table 1 of [16]. Here, in the last column of Table 9, we quote the original numbers for $g_{\rm A}(\beta\beta)$ produced in the IBA-2 calculations of [15]. The first two numbers refer to the use of the single-state dominance (SSD) hypothesis in the IBA-2 calculations. Based on the present analysis this assumption is approximately valid since, as discussed in Section 4, the magnitudes of the first 1^+ contribution and the final $2\nu\beta\beta$ NME are practically the same for the decays of ^{100}Mo (for small values of $g_{\rm A}$!) and ^{116}Cd.

The last number of the IBA-2 column in Table 9 refers to the assumption of closure approximation (CA) in the IBA-2 calculation. It is well established that such an approximation does not work for the $2\nu\beta\beta$ decays and thus this number could be dubious. Indeed, in a later publication [48] a more consistent theoretical framework was used (the interacting boson–fermion–fermion model, IBFFM-2) and in the case of $A = 128$ values of $g_{\rm A}$ were obtained that differ notably from the one obtained in [15]. These new, IBFFM-2 based values are presented in columns 5 and 6 of Table 9. One can see that the IBFFM-2 values of $g_{\rm A}(\beta)$ and $g_{\rm A}(\beta\beta)$ are very close to those of the present pnQRPA based calculations.

Based on the present results it is hard to judge if the trends of $g_{\rm A}(\beta)$ and $g_{\rm A}(\beta\beta)$ with increasing A are really there. In the shell-model calculations the trend of the effective value of $g_{\rm A}$ is much smoother in terms of A [15], as it is also for IBA-2, as shown in the last column of Table 9. Something very interesting occurs when one uses, instead of the varying values of $g_{\rm A}(\beta)$ and $g_{\rm A}(\beta\beta)$, the average values

$$\langle g_{\rm A}(\beta)\rangle = 0.57 \pm 0.21, \qquad \langle g_{\rm A}(\beta\beta)\rangle = 0.61 \pm 0.20, \tag{12}$$

obtained from Table 9. Indeed, the average values of the two effective $g_{\rm A}$ are compatible with each other, which is quite interesting. Thus it could be that the best way to interpret the present results is to adopt a common averaged value of

$$\langle g_{\rm A}\rangle \approx 0.6 \pm 0.2 \tag{13}$$

for the effective $g_{\rm A}$, to be used for both the beta and double beta calculations. The corresponding average from the work [56] would be $\langle g_{\rm A}\rangle \sim 0.66$, very close to the presently obtained average. Also the shell-model value [26] $\langle g_{\rm A}\rangle_{\rm SM} \sim 0.7$ is not far from that of (13).

The apparently larger quenching factor in the pnQRPA than in the shell-model could be attributed to missing the contributions of the complex configurations beyond the two-quasiparticle (particle–hole) configurations of the pnQRPA (see also [17]). On the other hand, it was shown in [57] for the $2\nu\beta\beta$ decay of ^{76}Ge and in [58] for the $2\nu\beta\beta$ decay of ^{100}Mo that the inclusion of the four-quasiparticle (two-particle–two-hole) degrees of freedom in a higher-QRPA scheme (in this case the pnMAVA) does not affect appreciably the low-energy Gamow–Teller properties of pnQRPA.

A degree of freedom missing in the present approach is the deformation. In [9] a deformed BCS + QRPA framework was used based on either a deformed Woods–Saxon or Hartree–Fock mean field. The Skyrme force Sk3 was used as the two-body interaction to describe the $2\nu\beta\beta$ decays of the $A = 48$–150 nuclei. There effective values $g_{\rm A} = 0.87$–1.0 were used in the calculations. It was found that the deformation affects, e.g., the $2\nu\beta\beta$ properties of the $A = 100$–128 nuclei although the involved deformations (see [9]) are not very large. This could have an impact also on the present results. In particular, the difference in deformation between the $2\nu\beta\beta$ initial and final nuclei can play a role. In [9] the β^- and EC decays of the first 1^+ states in the intermediate nuclei were not analyzed and consequently no tests of the adopted quenching factors were done from the point of view of beta decays. In fact, it would be highly interesting if a similar analysis as in the present work was done in the aforementioned deformed framework.

5.2. *Effective strength functions*

It is instructive to see how are the Gamow–Teller strength distributions and the cumulative $2\nu\beta\beta$ NMEs when the parameter $g_{\rm pp}$ resides within the ranges quoted in the second column of Table 9. All this information has been collected in Tables 10–12 for the studied nuclei. In the captions we specify the values of $g_{\rm pp}$ and $g_{\rm A}$. In these tables the calculated Gamow–Teller strengths, namely the (p, n) type of strength for transitions ^{100}Mo $\rightarrow$ ^{100}Tc, ^{116}Cd $\rightarrow$ ^{116}In and ^{128}Te $\rightarrow$ ^{128}I, and the (n, p) type of strengths for transitions ^{100}Ru $\rightarrow$ ^{100}Tc, ^{116}Sn $\rightarrow$ ^{116}In and ^{128}Xe $\rightarrow$ ^{128}I are defined as

$$B(\mathrm{GT})_-(m) = \left[g_{\rm A}(\beta)\right]^2 \left| \left(1^+_m \middle\| \sum_k t^-_k \boldsymbol{\sigma}_k \middle\| 0^+_i\right) \right|^2, \tag{14}$$

$$B(\mathrm{GT})_+(m) = \left[g_{\rm A}(\beta)\right]^2 \left| \left(1^+_m \middle\| \sum_k t^+_k \boldsymbol{\sigma}_k \middle\| 0^+_f\right) \right|^2, \tag{15}$$

where 0^+_i (0^+_f) is the ground state of the initial (final) nucleus in the $2\nu\beta\beta$ decay and 1^+_m is the m:th 1^+ state in the intermediate nucleus of the $2\nu\beta\beta$ decay. These strength functions can be called "effective strength functions".

In Tables 10–12 the strengths $B(\mathrm{GT})_\pm$ are summed up within energy bins of 1 MeV width. In the tables we give the strength up to 15 MeV of 1^+ excitation energy which corresponds to a practically saturated cumulative $2\nu\beta\beta$ NME given in the last columns of the tables. This energy interval also contains practically all of the GTGR region on the $B(\mathrm{GT})_-$ side. The effective cumulative $2\nu\beta\beta$ NME is defined as

Table 10
The calculated (p, n) type (14) and (n, p) type (15) bin-wise strengths (columns 2 and 4, respectively), up to 15 MeV of excitation energy, for Gamow–Teller transitions to 1^+ states in ^{100}Tc. Comparison with the experimental bin-wise (p, n) strength distribution from [59] is given in column 3. The cumulative $2\nu\beta\beta$ NME (16) for the $A = 100$ system of isobars is given in the last column of the table. The quantities are computed for the parameter values $g_{\rm pp} = 0.829$, $g_{\rm A}(\beta) = 0.655$ and $g_{\rm A}(\beta\beta) = 0.800$.

Bin (MeV)	$B(\mathrm{GT})_-$		$B(\mathrm{GT})_+$	$M^{(2\nu)}_{\rm cumul}$
	Calc.	Exp. [59]		
0.0–1.0	0.940	0.411	0.483	0.305
1.0–2.0	0.000	0.072	0.000	0.305
2.0–3.0	0.000	0.114	0.000	0.305
3.0–4.0	0.200	0.37	0.232	0.275
4.0–5.0	0.216		0.052	0.264
5.0–6.0	1.128		0.148	0.249
6.0–7.0	0.807		0.005	0.247
7.0–8.0	1.669		0.015	0.236
8.0–9.0	0.203		0.010	0.234
9.0–10.0	0.019		0.002	0.233
10.0–11.0	0.330		0.013	0.230
11.0–12.0	12.78		0.018	0.207
12.0–13.0	0.829		0.003	0.210
13.0–14.0	0.410		0.027	0.212
14.0–15.0	0.034		0.010	0.211

$$M^{(2\nu)}_{\rm cumul} = \left[g_{\rm A}(\beta\beta)\right]^2 \sum_{m=1}^{B} M^{(2\nu)}\left(1^+_m\right), \tag{16}$$

where all 1^+ states below the upper bound B of each bin are to be included into the cumulative sum. In this way we are then building up the matrix element $g_{\rm A}^4 |M^{(2\nu)}|^2$ of Eq. (2) and the inverse of the $2\nu\beta\beta$ half-life is directly obtained by multiplying with a corresponding phase-space factor of Table 1.

From Table 10 one can see that below 5 MeV the strength $B(\mathrm{GT})_-(^{100}\mathrm{Mo} \rightarrow {}^{100}\mathrm{Tc})$ is concentrated in the first bin in the calculations whereas experimentally the strength is more evenly distributed between 0 and 4 MeV. The calculated strength is somewhat larger than the measured one below 4 MeV. The situation is different for the strength $B(\mathrm{GT})_-(^{128}\mathrm{Te} \rightarrow {}^{128}\mathrm{I})$ as shown in Table 12. There the theoretical total strength below 5 MeV is larger than the experimental one, but shifted to a somewhat higher energy than the measured one. The $B(\mathrm{GT})_-$ strength below 5 MeV of excitation is the largest of all cases for the transition $^{116}\mathrm{Cd} \rightarrow {}^{116}\mathrm{In}$. For the $A = 100$ and $A = 128$ systems the GTGR is very pronounced at around 11–12 MeV whereas for the $A = 116$ system the GTGR is widely spread. For the $A = 128$ system the strength $B(\mathrm{GT})_+(^{128}\mathrm{Xe} \rightarrow {}^{128}\mathrm{I})$ is very small whereas for the $A = 100$ and $A = 116$ systems the interval 0–1 MeV gathers a large amount of the $B(\mathrm{GT})_+$ strength. In addition, there is a considerable amount of $B(\mathrm{GT})_+$ strength between 3 MeV and 6 MeV of excitation in the $A = 100$ system.

From Table 11 one notices that the cumulative $2\nu\beta\beta$ NME for the $A = 116$ system is practically constant after the first 1^+ contribution. The final value of the NME is 0.114 and we can really speak about SSD [61]. From Table 12 it is evident that there is a step in the cumulative

Table 11
The calculated (p, n) type (14) and (n, p) type (15) bin-wise strengths (columns 2 and 3, respectively), up to 15 MeV of excitation energy, for Gamow–Teller transitions to 1^+ states in ^{116}In. The cumulative $2\nu\beta\beta$ NME (16) for the $A = 116$ system of isobars is given in the last column of the table. The quantities are computed for the parameter values $g_{\rm pp} = 0.515$, $g_{\rm A}(\beta) = 0.710$ and $g_{\rm A}(\beta\beta) = 0.608$.

Bin (MeV)	$B(\mathrm{GT})_-$	$B(\mathrm{GT})_+$	$M^{(2\nu)}_{\rm cumul}$
0.0–1.0	0.624	0.402	0.100
1.0–2.0	0.876	0.001	0.103
2.0–3.0	0.171	0.000	0.104
3.0–4.0	0.517	0.003	0.104
4.0–5.0	0.360	0.003	0.105
5.0–6.0	0.162	0.000	0.105
6.0–7.0	0.013	0.000	0.105
7.0–8.0	1.357	0.002	0.107
8.0–9.0	1.774	0.028	0.108
9.0–10.0	0.755	0.001	0.109
10.0–11.0	0.025	0.009	0.108
11.0–12.0	9.776	0.003	0.110
12.0–13.0	1.903	0.002	0.111
13.0–14.0	4.318	0.008	0.113
14.0–15.0	6.589	0.005	0.113

Table 12
The calculated (p, n) type (14) and (n, p) type (15) bin-wise strengths (columns 2 and 4, respectively), up to 15 MeV of excitation energy, for Gamow–Teller transitions to 1^+ states in ^{128}I. Comparison with the experimental bin-wise (p, n) strength distribution from [60] is given in column 3. The cumulative $2\nu\beta\beta$ NME (16) for the $A = 128$ system of isobars is given in the last column of the table. The quantities are computed for the parameter values $g_{\rm pp} = 0.530$, $g_{\rm A}(\beta) = 0.333$ and $g_{\rm A}(\beta\beta) = 0.400$.

Bin (MeV)	$B(\mathrm{GT})_-$		$B(\mathrm{GT})_+$	$M^{(2\nu)}_{\rm cumul}$
	Calc.	Exp. [60]		
0.0–1.0	0.165	0.177	0.016	0.0224
1.0–2.0	0.121	0.380	0.001	0.0254
2.0–3.0	0.068	0.270	0.001	0.0256
3.0–4.0	0.254	< 0.04	0.001	0.0279
4.0–5.0	0.649	< 0.04	0.070	0.0406
5.0–6.0	0.000		0.000	0.0406
6.0–7.0	1.345		0.038	0.0438
7.0–8.0	0.000		0.000	0.0438
8.0–9.0	0.000		0.000	0.0438
9.0–10.0	0.003		0.001	0.0439
10.0–11.0	0.415		0.001	0.0441
11.0–12.0	4.399		0.002	0.0433
12.0–13.0	0.496		0.002	0.0437
13.0–14.0	0.048		0.002	0.0437
14.0–15.0	0.304		0.001	0.0437

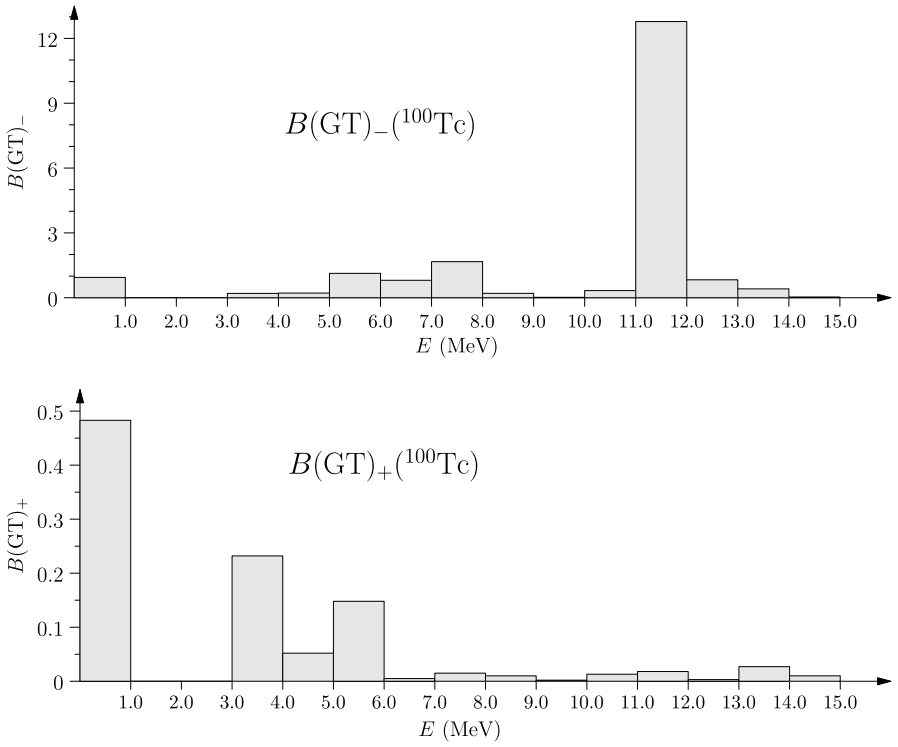

Fig. 8. Effective strength functions of (14) [upper panel] and (15) [lower panel] for Gamow–Teller transitions to 1^+ states in ^{100}Tc. The parameter values $g_{\mathrm{pp}} = 0.829$, $g_{\mathrm{A}}(\beta) = 0.655$ have been used.

NME at 4–5 MeV for the $A = 128$ system. The final value of the NME is 0.0442, not far from the last value of the cumulative NME quoted in Table 12. For the $A = 100$ system the NME is slowly decreasing and achieves its final value at 0.209, very close to the last value of the cumulative NME in Table 10.

To get a visual feeling of the effective strength functions they are presented separately in Figs. 8–10, where the upper panel relates to the $B(\mathrm{GT})_-$ strength (14) and the lower panel to the $B(\mathrm{GT})_+$ strength (15). As can be seen from the figures the $B(\mathrm{GT})_-$ strength looks qualitatively similar for $A = 100$ and $A = 128$ but for $A = 116$ the bulk of the strength is at a higher energy and the Giant resonance is more spread. For $A = 100$ and $A = 116$ the $B(\mathrm{GT})_+$ strength looks similar, except for $A = 116$ there is practically nothing beyond the first peak. For $A = 128$ there is relatively more $B(\mathrm{GT})_+$ strength at intermediate energies but the absolute strength is quite small as compared to the other two cases.

It is yet unclear what is the primary reason for the quenching of g_{A} and what is the share between the model-dependent and model-independent components of the quenching. The model-independent quenching can be associated with the non-nucleonic, i.e. isobaric degrees of freedom in nuclear matter [62,63]. The model-dependent quenching, associated with the limitations in the single-particle models space (ISM, IBA-2, IBFFM-2) or the lack of complicated many-nucleon configurations (pnQRPA, IBA-2, IBFFM-2) is certainly there and surprisingly enough the pnQRPA-based and the IBFFM-2 based formalisms seem to produce similar magnitudes of

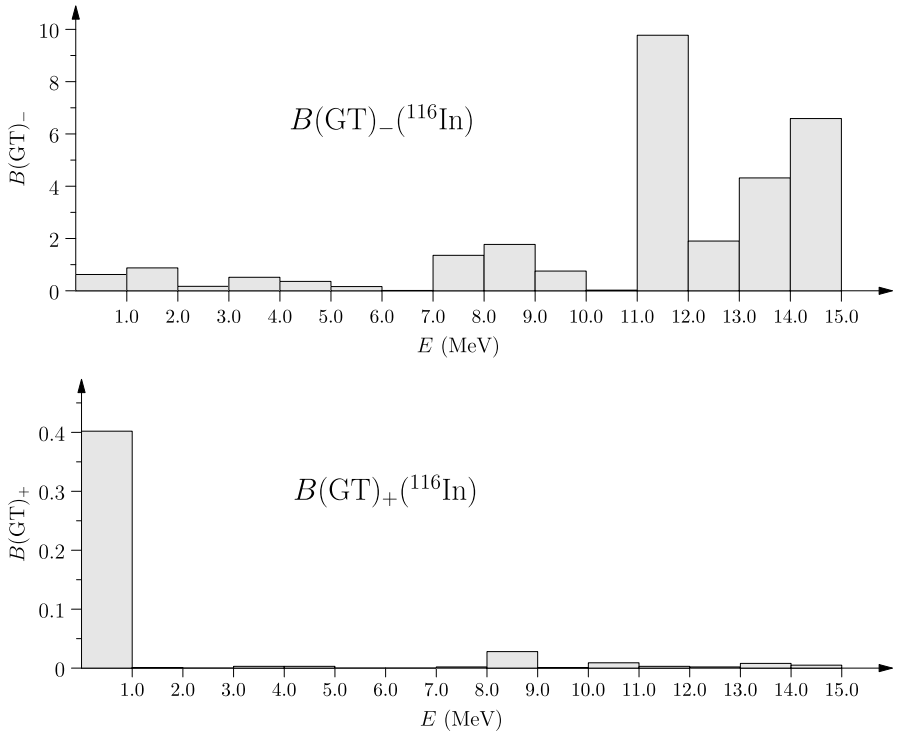

Fig. 9. Effective strength functions of (14) [upper panel] and (15) [lower panel] for Gamow–Teller transitions to 1^+ states in ^{116}In. The parameter values $g_{\rm pp} = 0.515$, $g_{\rm A}(\beta) = 0.710$ have been used.

quenching. The handling of quenching of $g_{\rm A}$ in different theory frameworks is an extremely interesting issue and certainly necessitates further investigation in the future.

6. Summary and conclusions

Two-neutrino double beta decays and single EC and β^- decays have been studied for the $A = 100$ (^{100}Mo–^{100}Tc–^{100}Ru), $A = 116$ (^{116}Cd–^{116}In–^{116}Sn) and $A = 128$ (^{128}Te–^{128}I–^{128}Xe) isobaric triplets in the framework of the proton–neutron quasiparticle random-phase approximation. The present calculations have been done in large single-particle model spaces with G-matrix based two-nucleon interactions. By examining the cumulative sums of the $2\nu\beta\beta$ NMEs we conclude that the three discussed isobaric systems behave differently in terms of cumulative contributions. By letting the value of the axial-vector coupling constant $g_{\rm A}$ vary freely, together with the particle–particle interaction strength parameter $g_{\rm pp}$, we can reproduce both the single and double beta decay data of a given isobaric triplet by using one value of $g_{\rm pp}$ and two values of $g_{\rm A}$, one for the single beta decays [$g_{\rm A}(\beta)$] and one for the double beta decay [$g_{\rm A}(\beta\beta)$]. The values of $g_{\rm A}(\beta)$ and $g_{\rm A}(\beta\beta)$ vary widely as functions of the mass number A. However, taking average values over A a common quenched value of $\langle g_{\rm A}\rangle \approx 0.6 \pm 0.2$ is arrived at. These findings may have drastic implications for the highly interesting $0\nu\beta\beta$ NMEs. The relation of our present results to the values of the $0\nu\beta\beta$ NMEs remains still an open issue but we view the present study as an incentive to tackle these issues in future investigations. Finally, it should be noted that in the

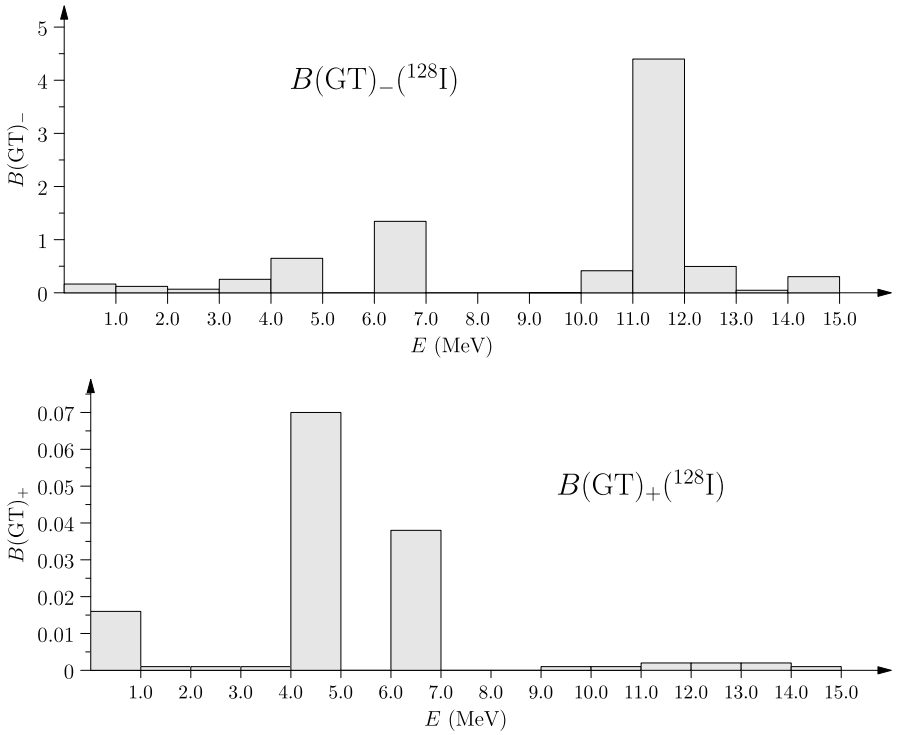

Fig. 10. Effective strength functions of (14) [upper panel] and (15) [lower panel] for Gamow–Teller transitions to 1^+ states in ^{128}I. The parameter values $g_{\mathrm{pp}} = 0.530$, $g_{\mathrm{A}}(\beta) = 0.333$ have been used.

present analysis we have used bare transition operators. In the case of a more advanced approach, using effective transition operators [64], the situation changes and part of the renormalization of g_{A} may be absorbed into these operators.

Acknowledgements

This work was supported by the Academy of Finland under the Finnish Center of Excellence Program 2012–2017 (Nuclear and Accelerator Based Program at JYFL) and by the CONICET of Argentina (PIP 5145 and PIP 112-200 801-00740).

References

[1] J. Suhonen, O. Civitarese, Weak-interaction and nuclear-structure aspects of nuclear double beta decay, Phys. Rep. 300 (1998) 123–214.
[2] J. Vergados, H. Ejiri, F. Šimkovic, Theory of neutrinoless double beta decay, Rep. Prog. Phys. 75 (2012) 106301.
[3] J. Suhonen, O. Civitarese, Double-beta-decay nuclear matrix elements in the QRPA framework, J. Phys. G, Nucl. Part. Phys. 39 (2012) 085105.
[4] J. Suhonen, O. Civitarese, Review of the properties of the $0\nu\beta^-\beta^-$ nuclear matrix elements, J. Phys. G, Nucl. Part. Phys. 39 (2012) 124005.
[5] J. Suhonen, O. Civitarese, Effects of orbital occupancies on the neutrinoless $\beta\beta$ matrix element of ^{76}Ge, Phys. Lett. B 668 (2008) 277–281.

[6] J. Suhonen, O. Civitarese, Effects of orbital occupancies and spin–orbit partners on $0\nu\beta\beta$-decay rates, Nucl. Phys. A 847 (2010) 207–232.
[7] J. Suhonen, Effects of orbital occupancies and spin–orbit partners II: $0\nu\beta\beta$ decays of ^{76}Ge, ^{82}Se and ^{136}Xe to first excited 0^+ states, Nucl. Phys. A 853 (2011) 36–60.
[8] J. Barea, F. Iachello, Neutrinoless double-β decay in the microscopic interacting boson model, Phys. Rev. C 79 (2009) 044301.
[9] R. Álvarez-Rodríguez, P. Sarriguren, E. Moya de Guerra, L. Pacearescu, A. Faessler, F. Šimkovic, Deformed quasiparticle random phase approximation formalism for single- and two-neutrino double β decay, Phys. Rev. C 70 (2004) 064309.
[10] E. Caurier, F. Nowacki, A. Poves, Nuclear-structure aspects of the neutrinoless $\beta\beta$-decays, Eur. Phys. J. A 36 (2008) 195–200.
[11] J. Menéndez, A. Poves, E. Caurier, F. Nowacki, Disassembling the nuclear matrix elements of neutrinoless $\beta\beta$ decay, Nucl. Phys. A 818 (2009) 139–151.
[12] T.R. Rodríguez, G. Martínez-Pinedo, Energy density functional study of nuclear matrix elements for neutrinoless $\beta\beta$ decay, Phys. Rev. Lett. 105 (2010) 252503.
[13] A. Faessler, G.L. Fogli, E. Lisi, V. Rodin, A.M. Rotunno, F. Šimkovic, Overconstrained estimates of neutrinoless double beta decay within the QRPA, J. Phys. G 35 (2008) 075104.
[14] J. Menéndez, D. Gazit, A. Schwenk, Chiral two-body currents in nuclei: Gamow–Teller transitions and neutrinoless double-beta decay, Phys. Rev. Lett. 107 (2011) 062501.
[15] J. Barea, J. Kotila, F. Iachello, Nuclear matrix elements for double-β decay, Phys. Rev. C 87 (2013) 014315.
[16] J. Suhonen, O. Civitarese, Probing the quenching of $g_{\rm A}$ by single and double beta decays, Phys. Lett. B 725 (2013) 153–157.
[17] J.D. Holt, J. Engel, Effective double-β-decay operator for ^{76}Ge and ^{82}Se, Phys. Rev. C 87 (2013) 064315.
[18] J. Suhonen, Nuclear matrix elements of $\beta\beta$ decay from β-decay data, Phys. Lett. B 607 (2005) 87–95.
[19] A.S. Barabash, Precise half-life values for two-neutrino double-β decay, Phys. Rev. C 81 (2010) 035501.
[20] J. Toivanen, J. Suhonen, Renormalized proton–neutron QRPA and its application to double beta decay, Phys. Rev. Lett. 75 (1995) 410–413.
[21] J. Toivanen, J. Suhonen, Study of several double-beta-decaying nuclei using the renormalized proton–neutron quasiparticle random-phase approximation, Phys. Rev. C 55 (1997) 2314–2323.
[22] A.A. Raduta, C.M. Raduta, A. Faessler, W.A. Kaminski, Description of the $2\nu\beta\beta$ decay within a fully renormalized RPA approach, Nucl. Phys. A 634 (1998) 497–524.
[23] C.M. Raduta, A.A. Raduta, Description of the $2\nu\beta\beta$ decay within a fully renormalized proton–neutron quasiparticle random-phase approximation with a restored gauge symmetry, Phys. Rev. C 82 (2010) 068501.
[24] E. Caurier, A. Poves, A.P. Zuker, A full $0\hbar\omega$ description of the $2\nu\beta\beta$ decay of ^{48}Ca, Phys. Lett. B 252 (1990) 13–17.
[25] A. Balysh, et al., Double beta decay of ^{48}Ca, Phys. Rev. Lett. 77 (1996) 5186–5189.
[26] E. Caurier, F. Nowacki, A. Poves, Shell model description of the $\beta\beta$ decay of ^{136}Xe, Phys. Lett. B 711 (2012) 62–64.
[27] P. Vogel, M.R. Zirnbauer, Suppression of the two-neutrino double-beta decay by nuclear-structure effects, Phys. Rev. Lett. 57 (1986) 3148–3151.
[28] O. Civitarese, A. Faessler, T. Tomoda, Suppression of the two-neutrino double β decay, Phys. Lett. B 194 (1987) 11–14.
[29] J. Suhonen, On the double-beta decays of ^{70}Zn, ^{86}Kr, ^{94}Zr, ^{104}Ru, ^{110}Pd and ^{124}Sn, Nucl. Phys. A 864 (2011) 63–90.
[30] V.A. Rodin, A. Faessler, F. Šimkovic, P. Vogel, Assessment of uncertainties in QRPA $0\nu\beta\beta$-decay nuclear matrix elements, Nucl. Phys. A 766 (2006) 107–131.
[31] M. Kortelainen, J. Suhonen, Improved short-range correlations and $0\nu\beta\beta$ nuclear matrix elements of ^{76}Ge and ^{82}Se, Phys. Rev. C 75 (2007), 051303(R).
[32] M. Kortelainen, J. Suhonen, Nuclear matrix elements of $0\nu\beta\beta$ decay with improved short-range correlations, Phys. Rev. C 76 (2007) 024315.
[33] J. Suhonen, M. Kortelainen, Nuclear matrix elements for double beta decay, Int. J. Mod. Phys. E 17 (2008) 1–11.
[34] J. Suhonen, From Nucleons to Nucleus: Concepts of Microscopic Nuclear Theory, Springer, Berlin, 2007.
[35] J. Kotila, F. Iachello, Phase-space factors for double-β decay, Phys. Rev. C 85 (2012) 034316.
[36] A. Bohr, B.R. Mottelson, Nuclear Structure, vol. I, Benjamin, New York, 1969.
[37] J. Suhonen, Opening of the $Z = 40$ sub-shell gap and the double beta decay of ^{100}Mo, Nucl. Phys. A 700 (2002) 649–665.
[38] D.R. Bes, O. Civitarese, J. Suhonen, Schematic and realistic model calculations of the isovector spin monopole (IVSM) excitations in ^{116}In, Phys. Rev. C 86 (2012) 024314.

[39] J. Suhonen, T. Taigel, A. Faessler, pnQRPA calculation of the β^+/EC quenching for several neutron-deficient nuclei in mass regions $A = 94$–110 and $A = 146$–156, Nucl. Phys. A 486 (1988) 91–117.
[40] J. Suhonen, Calculation of allowed and first-forbidden beta-decay transitions of odd–odd nuclei, Nucl. Phys. A 563 (1993) 205–224.
[41] D.R. Bes, O. Civitarese, Matrix elements for the ground-state $2\nu\beta\beta$ decay of Te isotopes in a hybrid model, Phys. Rev. C 81 (2010) 014315.
[42] B.P. Kay, et al., Valence neutron properties relevant to the neutrinoless double-β decay of ^{130}Te, Phys. Rev. C 87 (2013) 011302(R).
[43] F. Šimkovic, A. Faessler, P. Vogel, $0\nu\beta\beta$ nuclear matrix elements and the occupancy of individual orbits, Phys. Rev. C 79 (2009) 015502.
[44] J.P. Schiffer, et al., Nuclear structure relevant to neutrinoless double β decay: ^{76}Ge and ^{76}Se, Phys. Rev. Lett. 100 (2008) 112501.
[45] B.P. Kay, et al., Nuclear structure relevant to neutrinoless double β decay: the valence protons in ^{76}Ge and ^{76}Se, Phys. Rev. C 79 (2009) 021301(R).
[46] O. Civitarese, J. Suhonen, Is the single-state dominance realized in double-β-decay transitions?, Phys. Rev. C 58 (1998) 1535–1538.
[47] O. Civitarese, J. Suhonen, Systematic study of the single-state dominance in $2\nu\beta\beta$ decay transitions, Nucl. Phys. A 653 (1999) 321–337.
[48] N. Yoshida, F. Iachello, Two-neutrino double-β decay in the interacting boson–fermion model, Prog. Theor. Exp. Phys. 2013 (2013) 043D01.
[49] ENSDF at NNDC site, http://www.nndc.bnl.gov/.
[50] S. Sjue, et al., Electron-capture branch of ^{100}Tc and tests of nuclear wave functions for double-β decays, Phys. Rev. C 78 (2008) 064317.
[51] C. Wrede, et al., Electron-capture on ^{116}In and implications for nuclear structure related to double-β decays, Phys. Rev. C 87 (2013) 031303(R).
[52] B. Singh, Nuclear data sheets for $A = 128$, Nucl. Data Sheets 93 (2001) 33.
[53] A. Juodagalvis, D.J. Dean, Gamow–Teller GT$_+$ distributions in nuclei with mass $A = 90$–97, Phys. Rev. C 72 (2005) 024306.
[54] B.H. Wildenthal, M.S. Curtin, B.A. Brown, Predicted features of the beta decay of neutron-rich sd-shell nuclei, Phys. Rev. C 28 (1983) 1343–1366.
[55] G. Martínez-Pinedo, A. Poves, E. Caurier, A.P. Zuker, Effective g_A in the pf shell, Phys. Rev. C 53 (1996) R2602–R2605.
[56] A. Faessler, G.L. Fogli, E. Lisi, V. Rodin, A.M. Rotunno, F. Šimkovic, Overconstrained estimates of neutrinoless double beta decay within the QRPA, arXiv:0711.3996 [nucl-th].
[57] J. Kotila, J. Suhonen, D.S. Delion, Two-neutrino double beta decay of ^{76}Ge in an anharmonic vibrator approach, J. Phys. G 36 (2009) 045106.
[58] J. Kotila, J. Suhonen, D.S. Delion, Description of the two-neutrino $\beta\beta$ decay of ^{100}Mo by pnMAVA, J. Phys. G 37 (2010) 015101.
[59] J. Thies, et al., High resolution ^{100}Mo(^{3}He, t)^{100}Tc charge-exchange experiment and the impact on double-β decays and neutrino charged-current reactions, Phys. Rev. C 86 (2012) 044309.
[60] P. Puppe, et al., High resolution (^{3}He, t) experiment on the double-β decaying nuclei ^{128}Te and ^{130}Te, Phys. Rev. C 86 (2012) 044603.
[61] M. Bhattacharya, et al., Electron capture decay of ^{116}In and nuclear structure of double β decays, Phys. Rev. C 58 (1998) 1247–1256.
[62] A. Bohr, B.R. Mottelson, Nuclear Structure, vol. II, Benjamin, New York, 1975.
[63] A. Bohr, B.R. Mottelson, On the role of the δ resonance in the effective spin-dependent moments of nuclei, Phys. Lett. 100B (1981) 10–12.
[64] J. Suhonen, P. Divari, L. Skouras, I. Johnstone, Double beta decay of ^{92}Mo: Comparison of the shell model and the quasiparticle random-phase approximation, Phys. Rev. C 55 (1997) 714–719.